BMP, Tsuyama et al (20) found that the induced bone marrow cells are not the progeny of undifferentiated mesenchymal cells in situ, but rather arise from hematopoietic stem cells circulating in the peripheral blood. This conclusion was based on studies of chimeric mice and bone marrow transplantation (20).

In this diffusion chamber system, the cells within the chambers were able to survive by diffusion of tissue fluid from host animals, but vascular invasion was blocked by the filter membranes. As a result, the BMP-induced bone-forming reaction was stopped at the stage of cartilage formation and pieces of cartilage for transplantation were obtained, although it took a period of 5–6 weeks to achieve this outcome. This is a longer timeframe than the time taken by collagen pellets with rHuBMP-2 to form ectopic bone. In the ectopic endochondral bone formation process, ossification starts at the border of the cartilage and surrounding tissue.

The results of the RT-PCR analysis of type II collagen and aggrecan revealed that muscle-derived mesenchymal cells differentiated into chondrocytes at 4 days after implantation. However, mature cartilage matrix synthesis started a few days later, since the expression of type IX collagen, which is essential for type II collagen to form cartilage matrix, was weak at 4 days and increased significantly by day 7. Type X collagen and type XI collagen were detected by RT-PCR either with or without rHuBMP-2 in these cells. Because type II collagen and aggrecan were not detected initially, we cannot be sure that chondrogenesis started at the 0 time point. Further work will be needed to map out the exact sequence of expression of these genes in this model. In the absence of rHuBMP-2, the cells expressed type II collagen, but the level was much less when compared with that in cells with rHuBMP-2. This might mean that slow chondrogenesis of muscle-derived mesenchymal cells might occur even in the absence of rHuBMP-2 in this condition.

To examine whether osteogenic differentiation of the muscle-derived mesenchymal cells occurred in this system, we detected Cbfa1/Runx2, which is an essential transcriptional factor for osteoblastic differentiation, by RT-PCR. The expression of Cbfa1/Runx2 was observed at 96 hours in chambers with rHuBMP-2 but not observed in the absence of rHuBMP-2, which means that osteogenic differentiation was initiated by rHuBMP-2. We could not detect the expression of MyoD1 nor were there any cells showing a myogenic phenotype either in the chambers or in the defects at any time point.

The diffusion-chamber–engineered cartilage mass was able to repair full-thickness cartilage defects. At 24 weeks after transplantation, the transplanted cartilage was incorporated and effectively repaired the cartilage defects. The superficial layer of the transplant facing the joint surface had histologic characteristics of articular cartilage, but the greater part beneath the cartilage layer was replaced by bone mass, which was connected to the original subchondral bone. This morphologic condition suggests that part of the transplanted cartilage mass appeared to have features of preossifying cartilage and was in the process of remodeling. This adaptation to the surrounding environment also has been observed in an experiment involving cell transplantation to correct an osteochondral defect (13). When the cartilage plugs that were made in diffusion chambers were implanted into the osteochondral defects, they were replaced by bone from the bone marrow side, but the surface area that was in contact with the joint space remained as cartilage. We believe that the implanted chondrocytes remained at the surface of the defect, although there are no data to support this conclusion.

Adachi et al (21) reported that allogeneic muscle-derived cells embedded in collagen gels are useful for repair of full-thickness articular cartilage, both as a gene delivery vehicle and a cell source for tissue repair. They transduced rabbit allogeneic muscle-derived cells with the β-galactosidase gene (LacZ) and transplanted the cells into the osteochondral defects in the patellar groove in rabbit knees. They reported that the LacZ-positive cells were found in the defect only up to 4 weeks after transplantation. Further studies will be required to more completely understand the biochemical and morphologic processes that underpin the restorative actions of these cell and tissue transplants.

Although the generation of the new cartilage mass and repair of a cartilage defect with the engineered cartilage were shown to be successful in rats, there are some hurdles to be cleared before this approach can be applied in clinical practice. In this study, we used cells from the embryo, which were thought to be more primitive and to have greater capacity for differentiation. However, this represents a problem for clinical application, because of ethical and regulatory issues. Our technique could be applied to muscle-derived cells from the adult, and in this approach, we can use autologous cells. We are planning to apply this system to adult cells, such as bone marrow mesenchymal cells, adipocytes, and muscle-derived cells.

The less responsive nature of muscle-derived mesenchymal cells to rHuBMP-2 in large mammals, including humans, could also be an issue (22). Moreover, the optimal dose of BMP required for cartilage induc-

tion in humans must be determined. In order to solve these issues, further experimental studies in large animals will be essential.

The kinetics of BMP release from collagen is an important consideration. Sellers et al (23) reported that the mean residence time of rHuBMP-2 from a collagen sponge impregnated with 5 μg of rHuBMP-2 was 8 days, with an elimination half-life of 5.6 days. In addition, detectable amounts of rHuBMP-2 were present as long as 14 days after implantation.

In comparing the data from the present study with those reported by Sellers et al, there are differences in experimental details. Sellers et al implanted collagen with 5 μg of rHuBMP-2 into the osteochondral defect, which is likely to result in a rapid vascular invasion and much faster degradation. In the present study, collagen with 10 μg of rHuBMP-2 was placed into the chamber and implanted into subfascial pockets. The presence of the collagen in the chamber impeded invasion by the host cells. In addition, the preparation of a collagen gel and BMP-2 construct were different, and it would be reasonable to expect that the kinetics of BMP release would be influenced by these differences. It is also possible that the transplanted pellets might include BMP-2 at the time of implantation. Consequently, it would be the BMP-2, and not the cells in the pellet, that would drive the regeneration and the stability of repair cartilage. Further studies will be required to understand the kinetics of BMP release and the phenotypic stability of the transplanted cell population, which is believed to play a critical role in the outcome of tissue formation in vivo (24).

The present study has demonstrated another unique application of this approach, namely, the use of muscle-derived mesenchymal cells cultivated in an ex vivo system and differentiation of those cells into chondrogenic cells by rHuBMP-2 in diffusion chambers in an in vivo environment. Use of the muscle-derived mesenchymal cells together with rHuBMP-2 might be a reason for the successful generation of cartilage in this study, because these cells are known to have multilineage differentiation potential (21,25–27). While the present report provides evidence to support this approach for the successful treatment of articular cartilage defects, further studies will be needed to validate the technique for application in clinical practice.

REFERENCES

1. Buckwalter JA, Mankin HJ. Articular cartilage repair and transplantation. Arthritis Rheum 1998;41:1331–42.
2. Pridie KH. A method of resurfacing osteoarthritic knee joints. J Bone Joint Surg Br 1959;41:618–9.
3. Bert JM. Role of abrasion arthroplasty and debridement in the management of osteoarthritis of the knee. Rheum Dis Clin North Am 1993;19:725–39.
4. Steadman JR, Rodkey WG, Rodrigo JJ. Microfracture: surgical technique and rehabilitation to treat chondral defects. Clin Orthop 2001;391 Suppl:S362–9.
5. Hunziker EB. Articular cartilage repair: basic science and clinical progress [a review of the current status and prospects]. Osteoarthritis Cartilage 2002;10:432–63.
6. Matsusue Y, Yamamuro T, Hama H. Arthroscopic multiple osteochondral transplantation to the chondral defect in the knee associated with anterior cruciate ligament disruption. Arthroscopy 1993;9:318–21.
7. Jakob RP, Franz T, Gautier E, Mainil-Varlet P. Autologous osteochondral grafting in the knee: indication, results, and reflections. Clin Orthop 2002;401:170–84.
8. Chesterman PJ, Smith AU. Homotransplantation of articular cartilage and isolated chondrocytes: an experimental study in rabbits. J Bone Joint Surg Br 1968;50:184–97.
9. Grande DA, Pitman MI, Peterson L, Menche D, Klein M. The repair of experimentally produced defects in rabbit articular cartilage by autologous chondrocyte transplantation. J Orthop Res 1989;7:208–18.
10. Wakitani S, Kimura T, Hirooka A, Ochi T, Yoneda M, Yasui N, et al. Repair of rabbit articular surfaces with allograft chondrocytes embedded in collagen gel. J Bone Joint Surg Br 1989;71:74–80.
11. Kawamura S, Wakitani S, Kimura T, Maeda A, Caplan AI, Shino K, et al. Articular cartilage repair: rabbit experiments with a collagen gel-biomatrix and chondrocytes cultured in it. Acta Orthop Scand 1998;69:56–62.
12. Brittberg M, Lindahl A, Nilsson A, Ohlsson C, Isaksson O, Peterson L. Treatment of deep cartilage defects in the knee with autologous chondrocyte transplantation. N Engl J Med 1994;331:889–95.
13. Wakitani S, Goto T, Pineda SJ, Young RG, Mansour JM, Caplan AI, et al. Mesenchymal cell-based repair of large, full-thickness defects of articular cartilage. J Bone Joint Surg Am 1994;76:579–92.
14. Budenz RW, Bernard GW. Osteogenesis and leukopoiesis within diffusion-chamber implants of isolated bone marrow subpopulations. Am J Anat 1980;159:455–74.
15. Reddi AH. Cell biology and biochemistry of endochondral bone development. Coll Relat Res 1981;1:209–26.
16. Sasano Y, Ohtani E, Narita K, Kagayama M, Murata M, Saito T, et al. BMPs induce direct bone formation in ectopic sites independent of the endochondral ossification in vivo. Anat Rec 1993;236:373–80.
17. Kuboki Y, Saito T, Murata M, Takita H, Mizuno M, Inoue M, et al. Two distinctive BMP-carriers induce zonal chondrogenesis and membranous ossification, respectively; geometrical factors of matrices for cell-differentiation. Connect Tissue Res 1995;32:219–26.
18. Kronenberg HM. Developmental regulation of the growth plate. Nature 2003;423:332–6.
19. McKibbin B. The biology of fracture healing in long bones. J Bone Joint Surg Br 1978;60-B:150–62.
20. Tsuyama K, Takaoka K, Kitamura Y, Ono K. Origin of the marrow cells in bones induced by implantation of osteosarcoma-derived bone-inducing factor in mice. Clin Orthop 1983;172:251–6.
21. Adachi N, Sato K, Usas A, Fu FH, Ochi M, Han CW, et al. Muscle derived, cell based ex vivo gene therapy for treatment of full thickness articular cartilage defects. J Rheumatol 2002;29:1920–30.
22. Kawasaki K, Aihara M, Honmo J, Sakurai S, Fujimaki Y, Saka-

moto K, et al. Effects of recombinant human bone morphogenetic protein-2 on differentiation of cells isolated from human bone, muscle, and skin. Bone 1998;23:223–31.
23. Sellers RS, Zhang R, Glasson SS, Kim HD, Peluso D, D'Augusta DA, et al. Repair of articular cartilage defects one year after treatment with recombinant human bone morphogenetic protein-2 (rhBMP-2). J Bone Joint Surg Am 2000;82:151–60.
24. De Bari C, Dell'Accio F, Luyten FP. Failure of in vitro-differentiated mesenchymal stem cells from the synovial membrane to form ectopic stable cartilage in vivo. Arthritis Rheum 2004;50: 142–50.
25. Qu Z, Balkir L, van Deutekom JC, Robbins PD, Pruchnic R, Huard J. Development of approaches to improve cell survival in myoblast transfer therapy. J Cell Biol 1998;142:1257–67.
26. Lee JY, Qu-Petersen Z, Cao B, Kimura S, Jankowski R, Cummins J, et al. Clonal isolation of muscle-derived cells capable of enhancing muscle regeneration and bone healing. J Cell Biol 2000;150:1085–100.
27. Williams JT, Southerland SS, Souza J, Calcutt AF, Cartledge RG. Cells isolated from adult human skeletal muscle capable of differentiating into multiple mesodermal phenotypes. Am Surg 1999;65:22–6.

ELSEVIER

Bone 36 (2005) 399–407

BONE

www.elsevier.com/locate/bone

Low dose fibroblast growth factor-2 (FGF-2) enhances bone morphogenetic protein-2 (BMP-2)-induced ectopic bone formation in mice

Yukio Nakamura, Keiji Tensho, Hiroyuki Nakaya, Masashi Nawata, Takahiro Okabe, Shigeyuki Wakitani*

Department of Orthopaedic Surgery, Shinshu University School of Medicine, Asahi 3-1-1, Matsumoto 390-8621, Japan

Received 10 March 2004; revised 27 October 2004; accepted 4 November 2004

Abstract

To examine how fibroblast growth factor-2 (FGF-2) affects the BMP signaling pathway during bone morphogenetic protein-2 (BMP-2)-induced ectopic bone formation, we implanted type I collagen disks containing constant amounts of BMP-2 (5 μg) and varying amounts of FGF-2 onto the back muscles of adult male mice. We then performed histological analyses and histomorphometry, and measured bone mineral density and radiopaque area on the discs 1, 2, and 3 weeks after implantation. We also determined the expression profiles of several genes involved in bone formation and the BMP signaling pathway in the muscle that had been adjacent to the implanted disc and in muscle-derived primary culture cells that had similarly been treated with a constant concentration of BMP-2 and a varying concentration of FGF-2. In the presence of a constant amount of BMP-2, we confirmed that low doses of FGF-2 increased ectopic bone formation in vivo and high doses inhibited bone formation. Northern and/or Western blots of recovered muscle from the in vivo experiment and treated muscle-derived primary culture cells from the in vitro experiment revealed that low doses of FGF-2, but not high doses, increased the expression BMP receptor (BMPR)-1B, phosphorylated Smad1, Noggin, and Osteocalcin. Our results indicate that low-dose FGF-2 may facilitate BMP-2-induced ectopic bone formation by altering the expression of BMPRs on the surface of bone forming progenitor cells. They also indicate that the inhibitory effect of high-dose FGF-2 is not mediated via increased expression of the BMP inhibitor Noggin.

Keywords: Bone morphogenetic protein; Fibroblast growth factor; Ectopic bone formation

Introduction

Fibroblast growth factors (FGFs) comprise a family of multifunctional cytokines, with several family members affecting bone formation. Low doses of FGF-2 have been shown to increase bone morphogenetic protein (BMP-2)-induced ectopic bone formation, however, high doses of FGF-2 have been shown to inhibit this process [1–3]. The mechanism by which FGF-2 affects this process has not been delineated and is difficult to extrapolate from published studies which employed different FGF-2 doses and different models of bone formation. Consequently, we examined the effect of altering FGF-2 levels in a single model of ectopic bone formation that utilizes subcutaneously implanted BMP-2-containing collagen discs.

BMP-2, which is a member of the transforming growth factor-β (TGF-β) superfamily of secreted growth factors, has been shown to be a potent inducer of bone formation. For example, the implantation of BMP-2 with an appropriate carrier material consistently elicits local new bone formation in orthotopic and heterotopic sites [4–6]. BMPs signal through hetero-dimeric, membrane bound, serine-threonine kinase receptors, which in turn phosphorylate intracellular proteins (e.g., Smad-1 or -5) to effect intracellular signaling and physiological responses [7–11].

* Corresponding author. Fax: +81 263 35 8844.
E-mail address: wakitani@hsp.md.shinshu-u.ac.jp (S. Wakitani).

8756-3282/$ - see front matter © 2004 Elsevier Inc. All rights reserved.
doi:10.1016/j.bone.2004.11.010

In this report, we confirmed that FGF-2 affected the histology, histomorphometry, bone mineral density (BMD), and the radiopaque area of BMP-2-induced ectopic bone. We then showed that FGF-2 could alter the expression profile of genes/proteins that are associated with BMP signaling and bone formation in a dosage-dependent manner. Finally, we showed that these in vivo effects could be replicated in vitro using muscle-derived primary culture cells.

Materials and methods

Preparation of BMP-2 and FGF-2 retaining collagen discs

Recombinant human BMP-2 was produced by the Genetics Institute (Cambridge, MA) and donated to us through Yamanouchi Pharmaceutical Co. (Tokyo, Japan). The BMP-2 was provided in a buffer solution (5 m mol/l glutamic acid, 2.5% glycine, 0.5% sucrose, and 0.01% Tween-80) at a concentration of 1 μg/μl after filter sterilization [12]. FGF-2 was produced and donated to us through Kaken Pharmaceutical Co. (Tokyo, Japan). To prepare each implant sample, constant 5 μl (5 μg) of the BMP-2 solution was added into 15 μl of sterile water containing differing amounts of FGF-2 (0, 1, 10, 100 ng, and 1, 2.5, 5 μg), and all 20 μl were blotted into a porous collagen disk (6 mm diameter, 1 mm thickness) fabricated from commercially available bovine collagen sheets (Helistat, Integra Life Sciences Co., Plainsboro, NJ). The discs were then freeze-dried, and kept at −20°C until implantation into mice. These procedures were carried out under sterile conditions. The porous collagen disks with BMP-2 and FGF-2 were implanted onto the back muscles of mice.

Animal experimental protocols

This protocol was approved by the animal experimentation committee at Shinshu University School of Medicine. One hundred and sixty eight, 3-week-old male ddy mice were purchased from Nippon SLC Co. (Shizuoka, Japan) and housed in cages with free access to food and water for 1 week. Eight mice were used for each experimental group (i.e., differing FGF-2 dosage) and for each experimental time point (i.e., 1, 2, and 3 weeks following implantation). The discs were removed and analyzed for the following: BMD, the radiopaque area, the percentage of disc area containing bone, and the number of osteoclasts present. The discs were then stained with hematoxylin and eosin (HE) and Safranin-O. Muscle tissues surrounding the discs from four of every eight mice were used for Northern blotting while muscle tissues from remaining four mice were used for Western blotting.

Discs containing BMP-2 and FGF-2 were implanted subfascially onto the left back muscle of diethyl ether anesthetized mice. The incision site was stapled shut. One, 2, and 3 weeks later, discs were harvested from the mice following sacrifice with diethyl ether, by gently incising the skin and gently pulling out the disc using forceps. The BMD of each freshly recovered ossified disc (g/mm^2) was measured by single-energy X-ray absorptiometry using a bone mineral analyzer (Model DCS-600R, Aloka Co., Tokyo). The discs were then placed in 10% formalin for histologic analysis. The muscle underlying the disc was also harvested following sacrifice by cutting a slightly larger diameter circle than the disc. The muscle was then minced with scissors and used to recover total RNA and protein (methods described below). The average amount of muscle removed from each mouse was 165 ± 5.0 mg.

The radiopaque area in the radiograph of each implant was measured using a computer system with a scanner (Porascan 35 Ultra; Polaroid Co. Ltd., Cambridge, USA) and Photoshop software (Version 4.0J; Adobe Systems Inc., CA) and NIH-image (Version 1.61; National Institutes of Health, Bethesda, MD). Mean BMD or mean radiopaque area with Standard Deviation (SD) was obtained for the eight discs recovered from each treatment group of mice. Differences in the mean BMD or mean radiopaque are between experimental groups were evaluated with Dunnett's test.

Bone histomorphometric analysis

Following fixation in 10% formalin, the specimens were washed with 100 mM phosphate-buffered saline (PBS), and decalcified in 20% ethylene-diamine tetraacetic acid (EDTA). They were then dehydrated through graded ethanol and embedded in paraffin. Four μm thick cross-sections through the middle of each disc were processed for HE and Safranin-O staining. Photomicrographs of each cross-section were obtained and bone area (mm^2) was measured using NIH software. The percent of the total cross-sectional area that contains bone was also determined as was the total number of osteoclasts per section (number/slide). Differences in the mean bone area and the number of osteoclasts/slide between the experimental groups were evaluated with Dunnett's test.

Muscle-derived primary culture cell and measurement of cell number following exposure to BMP-2 and FGF-2

Muscle-derived primary culture cells were prepared from the thigh muscles of newborn ddy mice (Nippon SLC Co.), plated at a density of 2000 cells/well in a 96-well plate in 100 μl of serum free Dulbecco's modified Eagle's Medium (DMEM, Gibco-BRL, Grand Island, NY), and cultured for 24 h at 37°C in an atmosphere of humidified 5% CO_2. Cells were then switched to 100 μl of fresh DMEM containing 1 ng/μl of BMP-2 and differing concentrations of FGF-2 (0, 0.01, 0.1, 1, or 10 ng/μl). After 48 h, 10 μl of Cell Counting Kit-8 solution (Wako Pure Chemical Industries Ltd., Tokyo, Japan) was added into the plate, and incubated for 4 h at 37°C. The O.D. at 450 nm minus the O.D. at 620

nm was used to compare total cell numbers between the different groups. Each experiment was performed six times and the mean of the six experiments was compared between the different treatment groups using Dunnett's test.

Northern blot analysis of recovered muscle and muscle-derived primary culture cells

Total RNA from the retrieved back muscle that had been underlying the implanted discs and from the muscle-derived primary culture cells was extracted using an Isogen kit (Nippon Gene Co.) according to the manufacturer's instructions. Twenty micrograms of the total RNA were electrophoresed on a 1.0% agarose-formaldehyde gel and blotted onto a Hybond-N^+ membrane filter (Amersham Intl., NJ) for Northern blotting. Filters were hybridized overnight with random-primed [^{32}P]-labeled cDNA fragment probes representing BMPR-1A, -1B, -2, Noggin, osteocalcin (OC), Smad 6 or Runx2/cbfa1 at 65°C for 3 h in hybridization buffer (50 mM Tris–HCl: pH 7.5, 1 mg/ml denatured salmon sperm DNA, 1% sodium dodecyl sulphate, 1 M NaCl, 10 mM EDTA, 0.2% Ficoll 400, 0.2% polyvinylpyrolidone and 0.2% bovine serum albumin) and washed three times with 0.1× SSC and $NaSO_4$ for 1 h at 68°C. The signals were detected by a BioImaging Analyzer BAS-1500 (Fuji Photo Film Co., Tokyo, Japan). Gene expression was normalized to glyceraldehyde-3-phosphate dehydrogenase (GAPDH) levels. Membranes were re-used for different probes by boiling the membrane in 0.5% sodium dodecyl sulfate (SDS) between hybridizations.

Western blot analysis

Protein from the retrieved back muscle that had been underlying the implanted discs and muscle-derived primary culture cells were homogenized and mixed with an equal volume of 2× SDS sample loading buffer, boiled for 5 min in the presence of 5% β-mercaptoethanol. They were then centrifuged at 12,000 × *g*. The protein content of each supernatants was measured by a UV assay at an OD of 280 nm. Aliquots of supernatant were then adjusted to a concentration of 1 μg/μl, 5 μl were then mixed with 1 μl of 1% bromphenol blue, boiled for 2 min and electrophoresed through (10%–20%) SDS-PAGE gradient gels (35 mA, 90 min). Gels were then stained with Coomassie brilliant blue (CBB) (Sigma Co., St. Louis, MO) and then transferred to polyvinylidene difluoride (PVDF) membrane (Immunobilon-P Transfermembrane, Millipore, Bedford, MA) according to the manufacturer's instructions. Membranes were then treated with Blocking Reagent (Nippon Roche Co., Tokyo, Japan) for 1 h at room temperature, washed with PBS for 5 min, then incubated for 1 h with primary pSmad 1 or BMPRs antibody (1:100 dilution, Santa Cruz, San Diego, CA). After two 5-min washes with PBS, the membranes were incubated with peroxidase-conjugated rabbit anti-goat antibody (1:500 dil, Histofine, Nichirei Co., Tokyo, Japan) for 1 h. After two further 5-min washes with PBS, the reactive bands on the immunoblot were detected using ImmunoStar Kit for Rabbit (Wako Pure Chemical Industries Ltd.) and chemiluminescence.

This study was carried out in accordance with the World Medical Association Declaration of Helsinki.

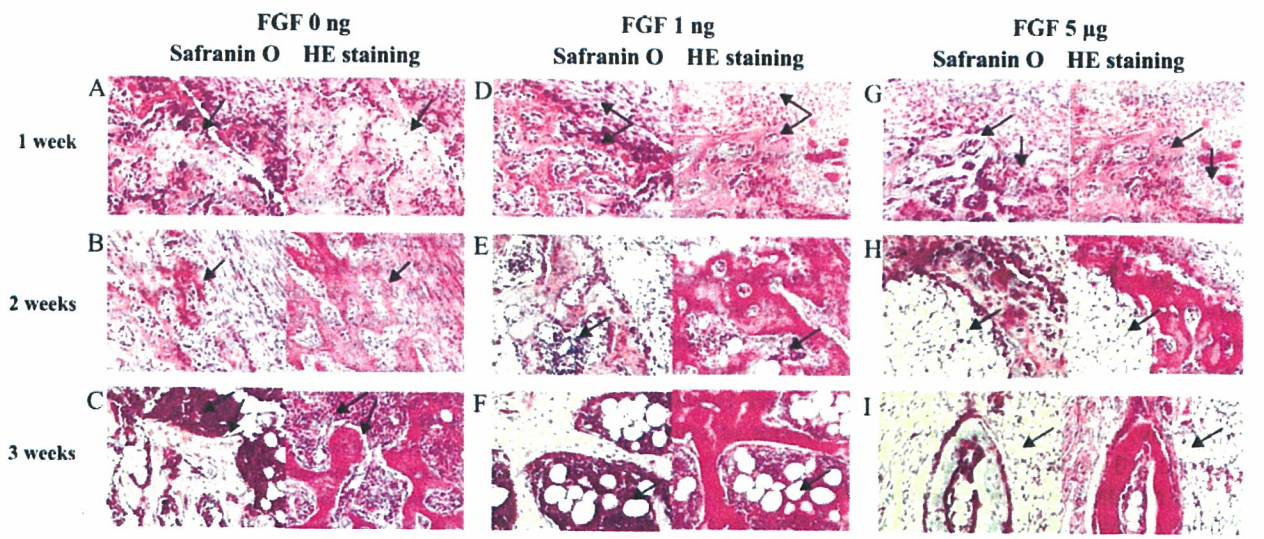

Fig. 1. Histologic analysis of BMP-2 and FGF-2 containing collagen discs and adjacent tissue retrieved 1–3 weeks after implantation onto the back muscles of mice. Representative sections (at 400× magnification) from the 0-ng FGF-2 (A–C), 1 ng FGF-2 (D–F), and 5 μg FGF-2 (G–I) containing discs are shown. For each sample, a Safranin-O-stained cross-section is in the left panel and a HE stained section is in the right panel. In discs containing 5 μg BMP-2 and no FGF-2, cartilage is present by 1 week (A, arrow), mineralizing bone is present at 2 weeks (B, arrow), and mature bone (C, arrow) with bone marrow (C, arrow) is present at 3 weeks. Discs containing 5 μg BMP-2 and 1 ng FGF-2 already have mineralizing bone at 1 week (D, arrow), and mature appearing bone (E, arrow) and bone marrow (E, arrow) by 2 weeks. By 3 weeks, there is extensive bone and bone marrow including adipocytes (F, arrow). Discs containing 5 μg each of BMP-2 and FGF-2, have less cartilage formation at 1 week (G, arrow), little mineralizing bone (H, arrow) but substantial adipocytosis (H, arrow) at 2 weeks, and little bone or bone mature appearing bone marrow at 3 weeks (I, arrow).

Results

Surgical survival and health of the mice following disc implantation

No mortality or adverse surgical outcomes (e.g., wound infection) occurred in any of the treatment groups. The health of all treated mice appeared unaffected by the disc implant as clinically assessed by weight gain and activity level.

FGF-2 has histologically detectable effects upon BMP-2-induced ectopic bone

In the absence of FGF-2, ectopic bone formed by BMP-2-induction followed a typical morphogenic pattern (Figs. 1A–C). After 1 week, cartilage had been formed adjacent to the disc (Fig. 1A). By 2 weeks, trabecular bone had begun to replace the cartilage (Fig. 1B). By 3 weeks, mature ectopic bone containing hematopoietic marrow cells and adipocytes was observed (Fig. 1C). Low doses of FGF-2 (1 or 10 ng) appeared to hasten and enhance bone formation compared to controls, since bone was present by 1 week (Fig. 1D), mature trabecular bone with bone marrow and adipocytes were recognizable by 2 weeks (Fig. 1E), and at 3 weeks, there was an increased amount of bone per high-power field (Fig. 1F). In contrast to the positive effects of low-dose FGF-2, high doses of FGF-2 (2.5 or 5 μg) did not appear to advance the timing of ectopic bone formation, since no bone was observable after 1 week (Fig. 1G). Furthermore, these amounts of FGF-2 reduced the amount of bone that was formed and increased the amount of adipose tissue (Figs. 1H–I) compared to the non-FGF-2-treated controls.

FGF-2 effects the BMD and radiopaque area of BMP-2-induced ectopic bone

Because FGF-2 treatment caused histologically detectable differences in ectopic bone formation, we measured BMD, radiopaque area, and the percent of the retrieved implants that were radiopaque to obtain more quantitative data (Figs. 2A–C). Similar to what we detected histologically, we observed that low doses of FGF-2 (1 and 10 ng) caused a statistically significant increase in the amount of ectopic bone that was formed around the implant while higher doses of FGF-2 (100 ng or greater) caused a statistically significant decrease in the amount of ectopic bone at 2 or 3 weeks, compared to controls (Figs. 2A–C). At 1 week, the BMD, the radiopaque area of the discs, and the percent of disc area containing bone were not different between the FGF-2-treated groups and the control groups. To determine whether the reduction in bone formation that occurs at higher doses of FGF-2 was due to diminished bone formation or increased bone resorption, we counted the number of osteoclasts per section and normalized that number to the bone area present in the section. As shown in Fig. 2D, the number of osteoclasts per unit radiopaque area

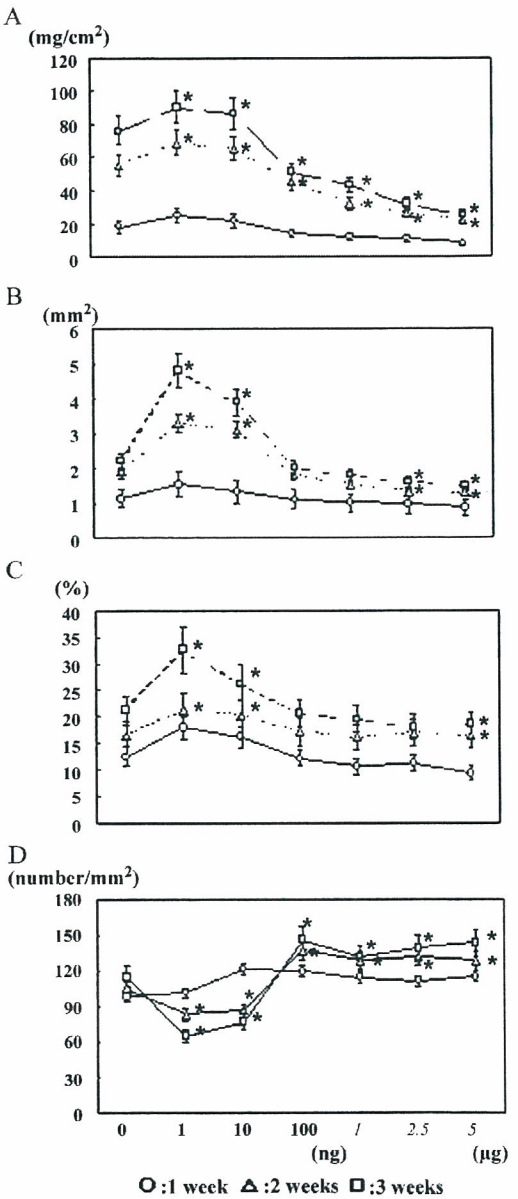

Fig. 2. Quantitative analysis of ectopic bone formation induced by BMP-2 and varying amounts of FGF-2. Compared to controls (i.e., 0 ng FGF-2), (A) the BMD of the discs was significantly increased ($P < 0.01$) in the 1- and 10-ng groups and significantly decreased ($P < 0.01$) in the 100 ng, and 1, 2.5 and 5 μg groups; (B) the radiopaque area of the discs was significantly increased ($P < 0.05$) in the 1- and 10-ng groups, and significantly decreased, in the 2.5- and 5-μg groups; (C) the percent of disc area containing bone was significantly increased in the 1 and 10 ng groups, and significantly decreased in the 5 ng group ($P < 0.05$); (D) the number of osteoclasts per disc was significantly decreased in the 1 and 10 ng groups ($P < 0.05$)and increased in the, but 100 ng, and 1, 2.5, and 5 μg groups ($P < 0.05$). Circles, triangles, and squares represent the discs recovered after 1, 2, and 3 weeks, respectively. * Indicates the value is significantly different from the control value at the specified P.

was not different between the high-dose group and the control group at 1 week. At 2 or 3 weeks compared to controls, low doses of FGF-2 (1 and 10 ng) cause a statistically significant decrease in the osteoclast number

while high doses of FGF-2 (100 ng or greater) cause a statistically significant increase the osteoclast number.

FGF-2 alters mRNA and protein expression in muscle adjacent to the implanted discs

Having confirmed that BMP-2-induced ectopic bone formation was increased by low dose FGF-2 and decreased by higher doses, we sought to determine the molecular mechanism for these effects by evaluating the expression profiles of several genes involved in the BMP-2 signaling pathway (Figs. 3A–G) in the adjacent muscle. We looked at the adjacent muscle assuming that it had provided many of the source cells for the ectopic bone.

Two heterodimeric membrane receptors, BMPR-1A/2 and BMPR-1B/2, bind to BMP-2 and can transduce signal.

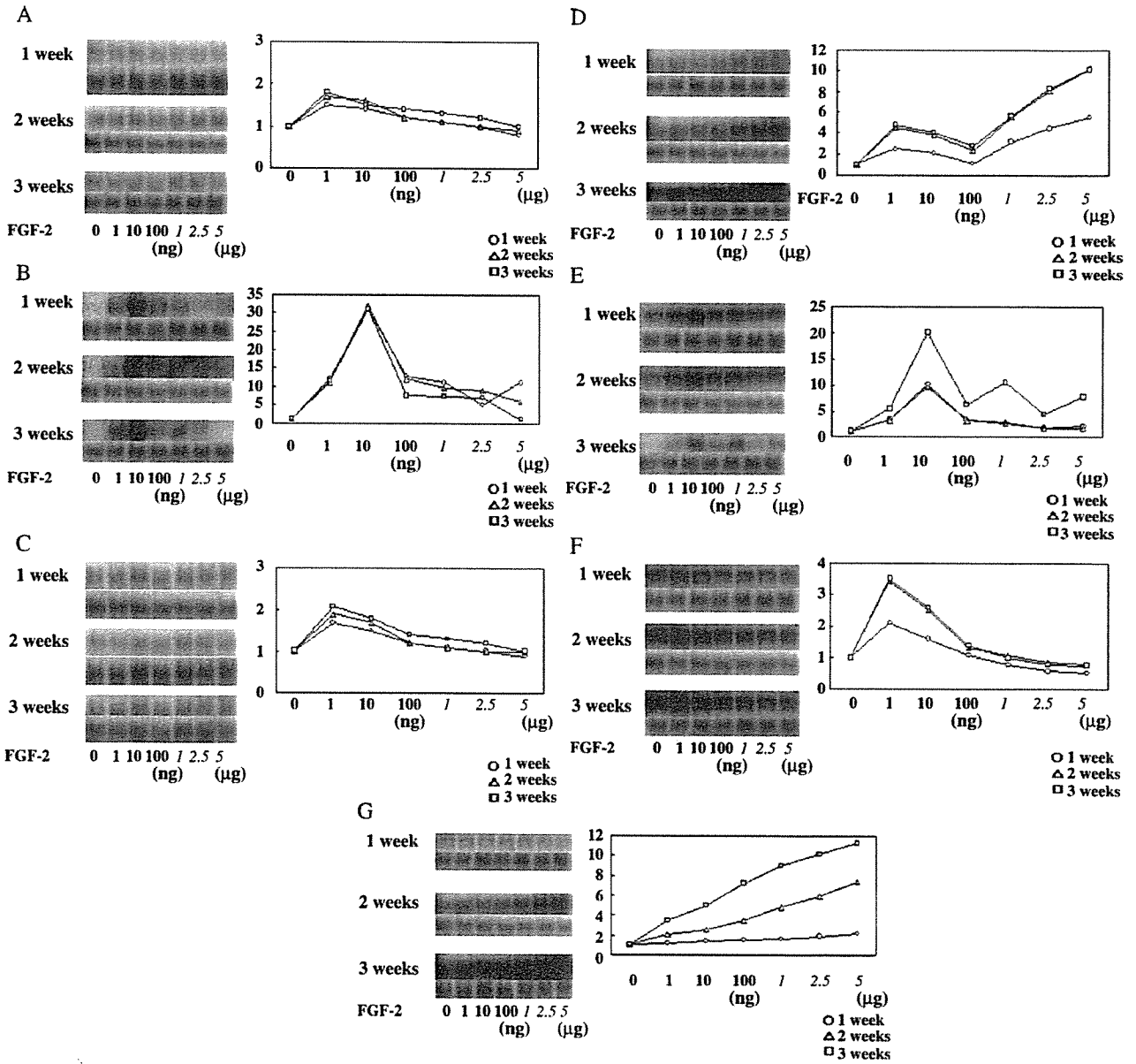

Fig. 3. Northern blot analysis in muscle underlying the implanted discs. (A) BMPR-1A. and (C) BMPR-2. In FGF-2 0 ng treated group, they were slightly increased, but decreased thereafter. (B) BMPR-1B was enhanced in low-dose FGF-2-treated groups, maximized in FGF-2 10 ng treated group, then decreased in high-dose FGF-2-treated groups. The tendencies of expression patterns were almost same at 1, 2, and 3 weeks after implantation. (D) Smad 6 was weekly induced in low-dose FGF-2-treated groups, enhanced in high-dose FGF-2-treated groups done dependently. The expression was more prominent 2 or 3 weeks than 1 week. (E) Noggin was induced in low-dose FGF-2-treated groups, maximized in the FGF-2 10 ng treated group, then decreased in high-treated FGF groups thereafter. The expression was most prominent 3 weeks after exposure to FGF-2 with BMP-2. (F) OC was maximally up-regulated in the FGF-2 1 ng treated group, then decreased dose dependently. The expression was more prominent 2 or 3 weeks than 1 week. (G) Runx2/cbfa1 was increased in a dosage manner. The expression was most prominent at 3 weeks, compared with 1 and 2 weeks. G3PDH mRNA levels obtained by Northern blotting were used for normalization. Quantitation of those factors mRNA levels was measured by Densitometry in each group. The score on day 0 was used as standard.

BMPR-1A and -2 mRNA level increased about double in the FGF-2-treated group, compared to control, however, a low level of expression was observed for each receptor subunit in response to the amount of 10, 100 ng, and 1, 2.5, and 5 μg FGF-2 or the number of weeks following the disc implant (Figs. 3A and C), suggesting that FGF-2 slightly affected this heterodimeric receptor. Western blotting showed that BMPR-1A and -2 were observed in the FGF-2-treated group at 1 or 2 weeks, but not at 3 weeks after implantation. However, BMPR-1A and -2 were not seen after stimulation to FGF-2. These results suggest that BMPR-1A and -2 might be differently regulated at the transcriptional and translational level during BMP-2-induced ectopic bone formation after exposure to FGF-2 (Figs. 4A and C). In contrast, the mRNA level for the receptor subunit BMPR-1B increased 10-fold to 30-fold increase in the FGF-2-treated group, respectively, compared to control (0 ng FGF-2) (Fig. 3B). This effect of FGF-2 on BMPR-1B mRNA was lost at higher doses. The expression of BMPR-1B at the protein level was also increased in low doses of FGF-2-treated groups, but lost at high doses (Fig. 4B).

To determine whether the increase in the BMPR-1B/2 receptor increased BMP signaling, we measured levels of pSmad 1 in the muscle using an antibody. Control and low-dose (1 and 10 ng) FGF-2-treated groups had greater amounts of pSmad 1 than the high-dose group at each time point, with differences between the low dose and control groups being most apparent at 3 weeks (Fig. 5).

Since BMP signaling can be inhibited by extracellular and intracellular BMP antagonists such as Noggin and

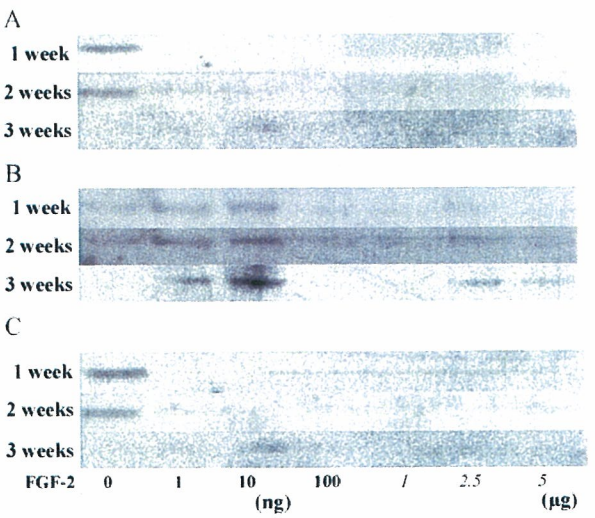

Fig. 4. Changes in BMP receptor expression in skeletal muscle underlying the implanted discs. Protein was extracted from recovered muscle, separated by SDS-PAGE reducing 10% PAGE and immunodetection using an (A) anti-BMPR-1A (B) anti-BMPR-1B, or (C) anti BMPR-2 antibody. Note that amounts of BMPR-1A and 2 are not detectable at all time points and do not vary with FGF-2 dose. In contrast, the amount of BMPR-1B was increased compared to control in the 1- and 10-ng FGF-2 groups; this is particularly apparent at the 3-week time point.

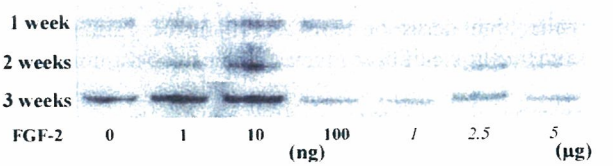

Fig. 5. Changes in the level of pSmad 1 in skeletal muscle underlying the implanted discs. Protein was extracted from recovered muscle, separated by SDS-PAGE reducing 10% PAGE and immunodetection using an anti-pSmad 1-specific antibody. Note the increased amounts of pSmad 1 in the groups, which is most apparent in the 2- and 3-week time points.

Smad 6, respectively, we looked at the effect of FGF-2 on the expression of these two mRNAs. Low doses had small effects upon Smad 6 expression, whereas high doses increased Smad 6 expression 2-fold to 12-fold over control (Fig. 3D). Surprisingly, FGF-2 levels had a different effect upon Noggin expression, with the 10 ng dose causing a nearly 20-fold increase in expression compared to control, while smaller and larger doses had only small effects (Fig. 3E). The increased expression of Noggin was much more prominent for low doses than high doses at 3 weeks, compared to 1 or 2 weeks after implantation (Fig. 3E).

To examine whether FGF-2 dose affects the expression of genes involved in osteogenesis, we measured the levels of the late stage osteoblast marker OC. OC mRNA was maximally induced by low dose FGF-2 (Fig. 3F). We also looked at expression of an early marker of osteoblast differentiation, Runx2/cbfa1, and found that FGF-2 increased its mRNA levels dose dependently (Fig. 3G).

FGF-2 has similar effects upon mRNA and protein expression in muscle-derived primary culture cells

The expression of BMPR-1B, Noggin, and OC mRNA in muscle-derived primary culture cells was increased at low FGF-2 concentrations (0.1 or 1.0 ng/ml) and decreased at higher concentrations (10 or 100 ng/ml). BMPR-1A or -2 mRNA expression was not altered by FGF-2. Smad 6 and Runx2/cbfa1 mRNA increased dose dependently (Fig. 6). Western blotting showed that pSmad 1 was increased by low concentrations of FGF-2 and decreased at high concentrations (Fig. 7). To determine whether FGF-2 increased bone formation by affecting the proliferation of osteoblast precursors, we counted the number of muscle-derived primary culture cells that had been exposed to varying levels of FGF-2. More cells were present following high-dose FGF-2 compared to low-dose FGF-2 indicating that increased bone formation in the presence of low-dose FGF-2 was not simply due to increased cell proliferation.

Discussion

A major challenge to the successful application of BMP in the clinic is that significant amounts of this protein are

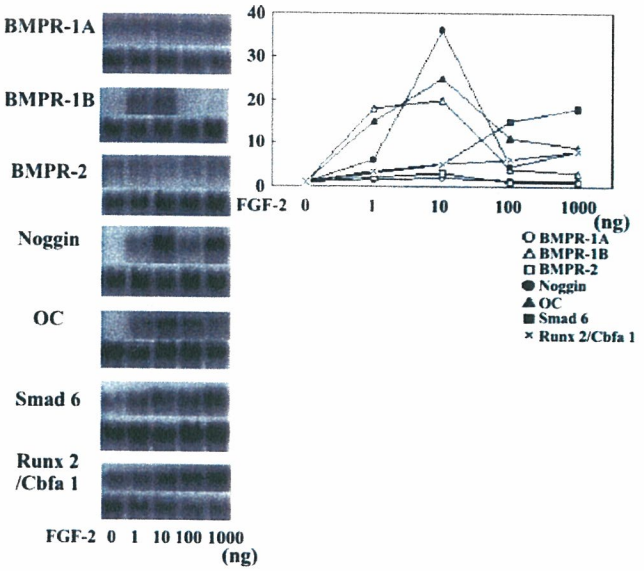

Fig. 6. Northern blot analysis in muscle-derived primary cell cultures treated with a constant amount of BMP-2 and varying concentrations of FGF-2. Note that the mRNA level of BMPR-1B was increased by low concentrations of FGF-2, and that the mRNA levels of BMPR-1A and 2 were unchanged by FGF-2. Also note the slight dose-dependent increases in Runx2/cbfa1 and Smad 6 expression. G3PDH mRNA levels obtained by Northern blotting were used for normalization. Quantitation of those factors mRNA levels was measured by Densitometry in each group. The score on day 0 was used as standard.

required for bone formation [13]. Therefore, combining anabolic agents that have synergistic effects is an attractive solution to this problem. Low-dose FGF-2 has previously been found to affect BMP-induced ectopic bone formation, which is that low-dose FGF-2 increased bone formation [1–3]. Ono et al. [3] demonstrated that a very small amount of FGF-2 has a strong promotive effect on the osteogenetic activity of BMP-2. Using implants in rats, Takita et al. [1] found that 100 ng of FGF-2 could enhance BMP-2 (0.8 μg)-induced ectopic bone formation whereas a higher dose (10 μg) exerted an inhibitory effect. Fujimura et al. [2] similarly showed in the presence of BMP-2 (2 μg) that low dose FGF-2 (0, 16, 80, and 400 ng) increased the radiopacity of implants whereas high-dose FGF-2 (2, 10, and 50 μg) was inhibitory. However, none of these studies looked at the mechanism underlying these dose-dependent effect. To begin to dissect the mechanism, we looked to see whether components of the BMP signaling pathway were affected differently by low-dose and high-dose FGF-2. Although our study utilized implants in mice, rather than rats, we also found that low dose FGF-2 enhanced BMP-2-induced bone formation whereas high-dose FGF-2 inhibited it.

Low dose FGF-2 caused increased mineral deposition as determined by DEXA and radiopaque area determination.

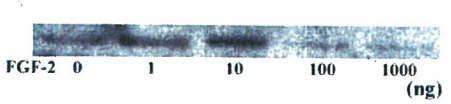

Fig. 7. Changes in the level of pSmad 1 in muscle-derived primary culture cells. Protein was extracted from recovered muscle, separated by SDS-PAGE reducing 10% PAGE and immunodetection using an anti-pSmad 1-specific antibody. pSmad 1 was induced dose dependently, maximized at the dose of 10 ng, then decreased at 100 or 1000 ng of FGF-2.

It also appears to hasten the rate of bone formation since a mature appearing marrow space within the ectopic trabecular bone occurs earlier than in control samples as shown by Fig. 1. Further evidence supporting a role for low-dose FGF-2 in bone formation derives from mRNA studies which indicate increased amounts of OC, which is a specific bone anabolic factor produced by osteoblasts [15] in the low-dose samples compared to controls as shown by Fig. 3F. In contrast, higher doses of FGF-2 resulted in less ectopic bone formation had been formed compared to controls.

Studies of mRNA and protein expression in muscle adjacent to the implanted discs and in muscle-derived primary culture cells exposed to constant BMP-2 and varying levels of FGF-2 suggest mechanisms for the dose-dependent effects. Most intriguing are the dose-dependent changes in expression of BMPR-1B mRNA and protein. BMP-2 signaling occurs through heterodimeric protein receptors [7–12]. We reported previously that BMPR-2 and -1A, but not BMPR-1B, were induced by BMP-2 alone during ectopic bone formation. These data suggested that BMPR-2 and -1A might be sufficient for BMP-2-induced ectopic bone formation [12]. However, the present data suggest FGF-2 may potentiate bone formation by inducing BMPR-1B expression thereby altering the BMP receptor profile on cells that are being recruited to this process. Additional support for this hypothesis derives from the observation that high doses of FGF-2 did not increase the expression of this receptor and did not enhance BMP-2-induced bone formation. Further evidence that low-dose, but not high-dose, FGF-2 potentiates BMP-2 signaling was seen in measures of pSmad 1 protein and Noggin mRNA expression. Smad 1 is a major downstream effector in the

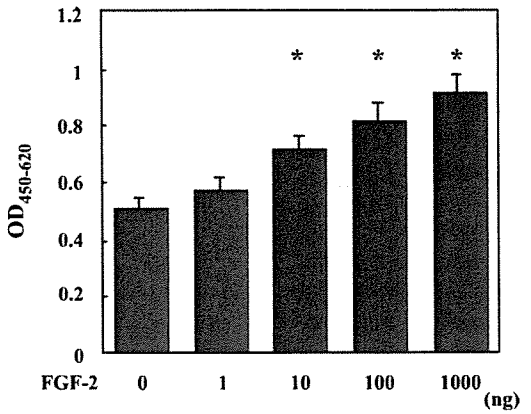

Fig. 8. Changes of cell numbers in muscle-derived primary culture cells after exposure to FGF-2 with a constant amount of BMP-2 (100 ng). The number of the cells significantly increased dose dependently in FGF-2 10, 100, and 1000 ng treated groups ($P < 0.05$).

BMP signaling pathway [16]. Noggin is an efficient inhibitor of BMP signaling [17–20]. We previously reported that Noggin was induced by BMP-2 during the formation of ectopic bone [12]. We confirm this in the present study and also show that Noggin expression is further enhanced by low-dose FGF-2. Our in vitro studies of muscle-derived primary culture cells (Figs. 6–8) also agree with our in vivo data that low-dose, but not high-dose, FGF-2 increases the expression of Noggin mRNA. It may seem paradoxical that increased levels of Noggin were found in tissue that had the highest amount of ectopic bone; however, this finding is consistent with increased BMP-2 signaling, since BMP has previously been shown to regulate Noggin expression via an autocrine loop [20]. Our results also indicate that the inhibitory effect of high-dose FGF-2 on BMP-2-induced bone formation is not via increase expression of Noggin.

Using cultured calvarial cells, Warren et al. [14] found that increasing concentrations of FGF-2 (2.5–40 ng) in the presence of a constant amount of BMP-4 (100 ng) suppressed Noggin expression in a dose dependent manner. Although this effect may explain the action of FGF-2 on cranial suture closure, it does not explain the effect of FGF-2 on ectopic bone formation in our model system. It remains to be determined whether these differing results are due to the cell types employed (calvarial cells versus muscle-derived primary culture cells), the BMP utilized (BMP-4 versus BMP-2), or the source of FGF-2.

We suspect that induction of BMPR-1B expression may account for the potentiation of low dose FGF-2 on bone induction; however, it cannot account for the inhibitory effects of high-dose FGF-2 on this process. Although we did not look at all extracellular inhibitors of BMP-2 signaling, Noggin was not induced by high levels of FGF-2. Consequently, we sought to determine whether high-dose FGF-2 might inhibit BMP-2 signaling via alternative intracellular mechanisms. We found that mRNA levels of the intracellular inhibitory Smad, Smad 6 [16], had a dose-dependent increase in response to FGF-2. Although we do not yet know whether this increase is physiologically relevant, it could provide an explanation for how high-dose FGF-2 inhibits bone formation without affecting expression of the BMPRs or the levels of pSmad 1. We also cannot preclude increased bone degradation as another cause of diminished BMD in the high-dose cohort since osteoclast number per total bone area was greater in the high-dose FGF-2 implants than in control.

The dose dependent effect of FGF-2 on Runx2/cbfa1 expression remains puzzling. The transcription factor Runx2/cbfa1 is essential to osteoblast differentiation but is also expressed in a number of other cell types, such as chondrocytes [10]. Although we found that Runx2/cbfa1 expression increased as the dose of FGF-2 increased, it did not correlate with the amount of ectopic bone that was formed in this study and therefore, may represent expression by non-osteoblastic cell types. We also found the FGF-2 increased cell number of muscle-derived primary culture cells in a dose-dependent manner. Therefore, the increased amount of bone induced in the presence of low-dose FGF-2 is unlikely to solely reflect enhanced proliferation of precursor cells.

The murine implant model we developed enables us to test for synergistic actions of growth promoting agents on bone formation. Using this model, we confirmed that low-dose FGF-2, but not high-dose FGF-2, could enhance BMP-2-induced ectopic bone formation. Our results further indicate that FGF-2 induced alterations in BMPR-1B expression contributed to this effect. Further delineation of this mechanism and optimal dosing in which FGF-2 acts synergistically with BMP-2 to enhance bone formation will hasten the therapeutic application of combination therapy.

Acknowledgment

We would like to thank Matthew L. Warman, an Associate Professor of Genetics and Pediatrics at Case Western Reserve University School of Medicine, for his critical reading of this manuscript and his suggestions to improve its clarity.

References

[1] Takita H, Tsuruga E, Ono I, Kuboki Y. Enhancement by bFGF of osteogenesis induced by rhBMP-2 in rats. Eur J Oral Sci 1997;105: 588–92.

[2] Fujimura K, Bessho K, Okubo Y, Kusumoto K, Segami N, Iizuka T. The effect of fibroblast growth factor-2 on the osteoinductive activity of recombinant human bone morphogenetic protein-2 in rat muscle. Arch Oral Biol 2002;47:577–84.

[3] Ono I, Tateshina T, Takita H, Kuboki Y. Promotion of the osteogenetic activity of recombinant human bone morphogenetic protein by basic fibroblast growth factor. J Craniofacial Surg 1996;7:418–25.

[4] Aspenberg P, Turek T. BMP-2 for intramuscular bone induction: effect in squirrel monkeys is dependent on implantation site. Acta Orthop Scand 1996;67:3–6.
[5] Itoh H, Ebara S, Kamimura M, Tateiwa Y, Kinoshita T, Yuzawa Y, et al. Experimental spinal fusion with use of recombinant human bone morphogenetic protein 2. Spine 1999;24:1402–5.
[6] Takaoka K, Yoshikawa H, Hashimoto J, Ono K, Matsui M, Nakazato H. Transfilter bone induction by Chinese hamster ovary (CHO) cells transfected by DNA encoding bone morphogenetic protein-4. Clin Orthop 1994;300:269–73.
[7] Miyazono K, Ichijo H, Heldin CH. Transforming growth factor-beta: latent forms, binding proteins and receptors. Growth Factors 1993;8:11–22.
[8] Fujii M, Takeda K, Imamura T, Aoki H, Sampath TK, Enomoto S, et al. Roles of bone morphogenetic protein type I receptors and Smad proteins in osteoblast and chondroblast differentiation. Mol Biol Cell 1999;10:3801–13.
[9] Ishidou Y, Kitajima I, Obama H, Maruyama I, Murata F, Imamura T, et al. Enhanced expression of type I receptors for bone morphogenetic proteins during bone formation. J Bone Miner Res 1995:1651–9.
[10] Onishi T, Ishidou Y, Nagamine T, Yone K, Iamamura T, Kato M, et al. Distinct and overlapping patterns of localization of bone morphogenetic protein (BMP) family members and a BMP type II receptor during fracture healing in rats. Bone 1998;22:605–12.
[11] Kaneko H, Arakawa T, Mano H, Kaneda T, Ogasawara A, Nakagawa M, et al. Direct stimulation of osteoclastic bone resorption by bone morphogenetic protein (BMP)-2 and expression of BMP receptors in mature osteoclasts. Bone 2000;27:479–86.
[12] Nakamura Y, Wakitani S, Nakayama J, Wakabayashi S, Horiuchi H, Takaoka K. Temporal and spatial expression profiles of BMP receptors and noggin during BMP-2-induced ectopic bone formation. J Bone Miner Res 2003;18:1854–62.
[13] Saito N, Okada T, Horiuchi H, Murakami N, Takahashi J, Nawata M, et al. A biodegradable polymer as a cytokine delivery system for inducing bone formation. Nat Biotechnol 2001;19: 332–5.
[14] Warren SM, Brunet LJ, Harland RM, Economides AN, Longaker MT. The BMP antagonist noggin regulates cranial suture fusion. Nature 2003;422:625–9.
[15] Desbois C, Karsenty G. Osteocalcin cluster: implications for functional studies. J Cell Biochem 1995;57:379–83.
[16] Miyazono K. Signal transduction by bone morphogenetic protein receptors: functional roles of Smad proteins. Bone 1999;25:91–3.
[17] Holley SA, Neul JL, Attisano L, Wrana JL, Sasai Y, O'Connor MB, et al. The *Xenopus* dorsalizing factor noggin ventralizes *Drosophila* embryos by preventing DPP from activating its receptor. Cell 1996;86:607–17.
[18] Zimmerman LB, De Jesus-Escobar JM, Harland RM. The Spemann organizer signal noggin binds and inactivates bone morphogenetic protein 4. Cell 1996;86:599–606.
[19] Ito H, Akiyama H, Shigeno C, Nakamura T. Bone morphogenetic protein-6 and parathyroid hormone-related protein coordinately regulate the hypertrophic conversion in mouse clonal chondrogenic EC cells, ATDC5. Biochem Biophys Res Commun 1999;260:240–4.
[20] Gazzerro E, Gangji V, Canalis E. Bone morphogenetic proteins induce the expression of noggin, which limits their activity in cultured rat osteoblasts. J Clin Invest 1998;102:2106–14.

American Journal of Pathology, Vol. 167, No. 1, July 2005

Molecular Pathogenesis of Genetic and Inherited Diseases

Expression Profiles and Functional Analyses of Wnt-Related Genes in Human Joint Disorders

Yukio Nakamura,*† Masashi Nawata,* and Shigeyuki Wakitani*

From the Department of Orthopaedic Surgery, Shinshu University School of Medicine, Matsumoto, Japan; and the Department of Genetics,† Howard Hughes Medical Institute/Case Western Reserve University, Cleveland, Ohio*

Rheumatoid arthritis (RA) and osteoarthritis (OA) are joint disorders that cause major public health problems. Previous studies of the etiology of RA and OA have implicated Wnt genes, although the exact nature of their involvement remains unclear. To further clarify the relationship between RA, OA, and the Wnt gene family, gene expression analyses were performed on articular cartilage, bone, and synovial tissues in knee joints taken from RA, OA, and normal/control patients. Cytokine assays were also performed in cells transfected with Wnt-7b, a member of the gene family most closely linked to RA and OA. Of the human Wnt genes, real-time PCR analysis revealed significant up-regulation of Wnt-7b in OA cartilage and RA synovium. *In situ* hybridization and immunohistochemistry also revealed that Wnt-7b was present in articular cartilage, bone, and synovium of RA samples and in osteophytes, articular cartilage, bone marrow, and synovium of OA samples. The levels of the cytokines tumor necrosis factor-α, interleukin-1β, and interleukin-6 were significantly increased in RA synovium and Wnt-7b-transfected normal synovial cells when compared with normal samples. These results point to the potential involvement of Wnt signaling in the pathobiology of both RA and OA. *(Am J Pathol 2005, 167:97–105)*

Rheumatoid arthritis (RA) and osteoarthritis (OA) are two of the most common joint disorders in humans. RA is characterized by synovial inflammation, osteoporosis, generalized loss of cartilage, and bony erosions in joints that ultimately lead to significant disability of joint movement.[1] OA also can be defined as an organ-level failure of a diarthrodial joint, which is characterized radiographically by loss of joint space, subchondral sclerosis, bony contour remodeling, and the presence of osteophytes. Osteophytes represent areas of new cartilage and bone formation.[2,3] The prevalence of RA or OA is still increasing, and it is estimated that approximately 30 million people aged ≥35 years have RA or OA according to the Third National Health and Nutrition Examination Survey conducted by the National Center for Health Statistics from 1988 to 1994 in the United States.[4] However, the etiology of these destructive joint disorders has not been defined. Here, we analyzed molecular events in the joints using Japanese patients with destructive joint disorders.

Over the past few decades, the mechanisms involved in skeletal pattern formation have been clarified at the molecular level, due to the discovery and identification of diffusible factors that regulate skeletal morphogenesis. Of these factors, bone morphogenetic proteins (BMPs), fibroblast growth factors (FGFs). Hedgehog, and Wnts have received considerable attention in the pathomorphology research area. The involvement of these proteins in the formation, growth, maintenance, and turnover of the skeleton has been confirmed by a number of genetic studies.[5,6]

The Wnt gene was first defined as a proto-oncogene (int-1).[7,8] To date, 19 molecular types in the human Wnt family have been reported. Wnt signaling is transduced via the β-catenin-TCF pathway, the Ca^{2+}-releasing pathway, or the Jun-N-terminal kinase pathway.[9,10] The Wnt signal transduction system is involved in the determination of polarity, differentiation, and proliferation of zooblasts, and it regulates axial formation, organogenesis, carcinogenesis, embryogenesis, and morphogenesis.[11–13] Wnt genes also play a key role in the highly regulated processes of vertebrate skeletogenesis, endochondral bone formation, and fracture repair.[12,14–17] Wnt-1, -5a, -7a, and 9a (-14) are thought to inhibit the differentiation of undifferentiated mesenchymal cells into chondrocytes. Wnt-1, -3a, -4, -7a, and -7b also inhibit early differentiation of chondrocytes in the chick

Accepted for publication March 24, 2005

A related commentary by Y. Ishikawa appears in this issue (Am J Pathol 2005, 167: 1–3).

Address reprint requests to Shigeyuki Wakitani, M.D., Department of Orthopaedic Surgery, Shinshu University School of Medicine, Asahi 3-1-1, Matsumoto, 390-8621, Japan. E-mail: wakitani@hsp.md.shinshu-u.ac.jp.

limb.[13–20] In addition, these Wnt genes are associated with BMP signaling or synovial joint formation and the maintenance of joint integrity.[17,20] Recently, the importance of the Wnt pathway in normal bone accrual and in fibroblast-like cells in RA patients was reported.[16,19,21,22] However, the role of the Wnt signaling pathway in association with the onset and/or progress of destructive joint disease has not been fully established compared with other factors, such as BMPs, FGFs, and hepatocyte growth factors. This is due in part to the fact that increasing numbers of subtypes have been identified and added to the Wnt family. Therefore, a comprehensive analysis of Wnt gene family expression in the joint might provide useful insight into the role of Wnt family members in the pathophysiology of joint destruction.

In this setting, we compared quantitatively the expression level of all human Wnt genes reported so far in joint tissues from RA, OA, and normal/control patients, and we investigated the distribution of Wnt proteins in the joint tissues of these patients. We also examined the potential role of Wnt genes by performing human cytokine assays after transfection of Wnt-7b, the most significant gene in RA or OA in this study, into human joint tissues.

Materials and Methods

Patients

We used knees of RA or OA patients based on the criteria of American College of Rheumatology who underwent total knee arthroplasty (TKA). The condition of all samples was in the end stage of the diseases. As control tissues, knee joint tissues of knee injuries that underwent arthroscopies or hip tissues of femoral neck fracture that underwent bipolar hip replacement, were used. Articular cartilage, bone, and synovial tissue from three groups (OA group; RA group; control: non-RA, non-OA, but traumatic group) were removed surgically and processed rapidly to extract RNA. Patients experiencing complications were excluded from the study. Each subject involved in the study had signed informed consent before the operation. This study was carried out in accordance with the World Medical Association Declaration of Helsinki.

Tissue Collection and Processing for Reverse Transcribed-Polymerase Chain Reaction (RT-PCR)

RT-PCR was performed to analyze all human Wnt genes reported so far using samples from the following patient groups: 10 RA patients who underwent TKA varying in age from 27 to 72 years (male, 1; female, 9; averaged age, 53.1 years), 9 OA patients who underwent TKA varying in age from 43 to 81 years (male, 3; female, 6; averaged age, 66.6 years), and 7 trauma patients who underwent bipolar hip replacement varying in age from 32 to 82 years (male, 1; female, 6; averaged age, 65.1). PCR primers were checked by Blast, and their sequences were confirmed to be specific to the designated target.

Total RNA from fresh, rapidly frozen tissue samples was extracted using Isogen (Nippon Gene Co., Tokyo, Japan) according to the manufacturer's instructions. A portion of the cDNA mixture was used as a template for PCR using primer pairs specific for Human Wnts-1, -2, -3, -3a, -4, -5a, -5b, -6, -7a, -7b, -8a, -8b, -9a, -14, -9b, -15, -10a, -10b, -11, -13, -16, and FRZB. PCR products were separated on a 2% agarose gel. Each PCR product was subcloned and sequenced using a DNA sequencing kit (Applied Biosystems, Warrington, UK). The nucleotide sequences of the cloned PCR products were compared with those in the GenBank databases (GenBank Wnt-3:NM030753, Wnt-3a: XM047539, Wnt-4:NM030761, Wnt-5a:XM016181, Wnt-5b: XM053451, Wnt-7b:NM004625, Wnt-8b:XM005702, Wnt-10a:XM050840, Wnt-10b:XM053707, Wnt-11:XM006222, Wnt-13:AB070218, Wnt-14:NM003395, Wnt-15:NM003396, and Frzb:NM001463). Five or more RT-PCR reactions were run for a single gene in each joint tissue sample.

Tissue Collection and Processing for Real-Time PCR

Real-time PCR was performed to analyze human Wnts -3, -3a, -4, -5a, -5b, -7b, -8b, -10a, -10b, -11, -13, -14, -15 p-catenin, FRZB, and low-density lipoprotein receptor-related protein[5] (LRP5). The following tissues were completely different from the sample used by RT-PCR. Eight RA patients varying in age from 52 to 79 years (male, 1; female, 7; averaged age, 70.2 years), 11 OA patients varying in age from 72 to 94 years (male, 1; female, 10; averaged age, 84.4 years) who underwent TKA, and 11 trauma patients varying in age from 17 to 72 years (male, 5; female, 6; averaged age, 34.4 years) who underwent joint arthroscopies were selected for real-time PCR.

Tissue samples collected during the surgery were frozen immediately after removal and stored at −80°C in a freezer. For RNA preparations, the frozen tissues were crushed in the presence of liquid nitrogen and solubilized with TRIzol (Invitrogen, Tokyo, Japan) at room temperature for 30 minutes. After mixing with $CHCl_3$, the aqueous phase was separated by centrifugation and precipitated with isopropanol. The precipitated nucleic acids were dissolved in RNase-free water and then treated with DNase I (Qiagen, Tokyo, Japan). The concentration of the RNA obtained was determined by using the 2100 Bio-Analyzer (Agilent Technologies, Tokyo, Japan). cDNA was synthesized from 1 μg of total RNA with dT primer (Advantage RT for PCR kit; Clontech, Tokyo, Japan). TaqMan reactions were run using the TaqMan Universal PCR Master Mixture (PE Biosystems, Tokyo, Japan). The reaction conditions were as follows: 50°C for 2 minutes, 95°C for 10 minutes, followed by 94°C (15 seconds) and 60°C (1 minute) for 40 cycles. Using the real-time PCR method, the template concentration is determined by the Ct value. Ct or threshold cycle, is the PCR cycle at which an increase in reporter fluorescence above a baseline signal can first be detected. The glyceraldehyde-3-phos-

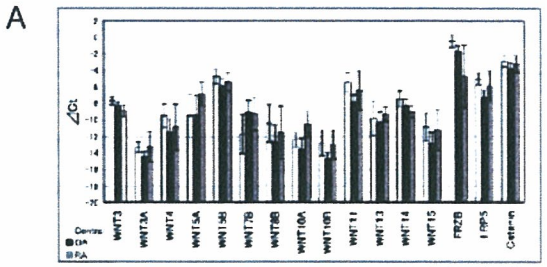

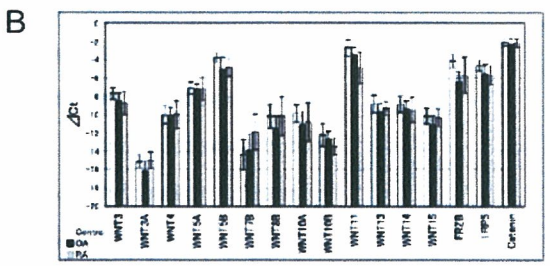

C

	OA Cartilage	OA Synovium	RA Cartilage	RA Synovium
Wnt-3			↓	↓
Wnt-3a		↓		
Wnt-5b	↓	↓		
Wnt-9a			↓	
Wnt-9b		↓		
Wnt-7b	↑			↑
Wnt-10a			↑	
Wnt-10b	↓			↓
Wnt-11	↓			↓
FRZB		↓	↓	↓

↑: increased, ↓: decreased, compared to control

Figure 1. Comprehensive analyses of Wnt genes, FRZB, LRP5, and β-catenin in human control samples, cartilage, and synovium in RA (**A**) and cartilage and synovium in OA (**B**) by real-time PCR. The template concentration is determined by the Ct value. GAPDH gene is used as an internal control. The abundance of each Wnt transcript is expressed as ΔCt, which is the difference between Ct (GAPDH) and Ct (target gene). The baseline of ΔCt is set at −20, so that more mRNA expressions correspond to longer bars. Expression pattern of Wnt genes by real-time PCR in RA, OA cartilage and synovium. **C:** Summary of the results in **A** and **B**. Wnt-7b in OA cartilage, and RA synovium, Wnt-10a in RA cartilage were significantly up-regulated, compared with control samples. Wnt-3 in RA cartilage and synovium, Wnt-3a in OA synovium, Wnt-5b in OA cartilage and synovium, Wnt-9a in RA cartilage, Wnt-9b in OA synovium, Wnt-10b in OA cartilage and RA synovium, Wnt-11 in OA cartilage and RA synovium, FRZB in OA synovium, and RA cartilage and synovium were significantly down-regulated compared with control samples.

phate dehydrogenase (GAPDH) gene is used as an internal control. The abundance of each Wnt transcript is expressed as ΔCt, which is the difference between Ct (GAPDH) and Ct (target gene). Because GAPDH is expressed abundantly, ΔCt has a negative value for all Wnt genes. In Figures 1 and 2, the baseline of ΔCt is set at −20, so more mRNA expressions correspond to longer bars. Sequences of primers and probes for the real-time PCR primers are described in Table 1.

We used the so-called $^{2\Delta\Delta Ct}$ method to analyze relative changes of Wnt-7b or -10a as described elsewhere by Livak et al.[23] The means ± SD of each Wnt gene, β-catenin, FRZB, and LRP5 expression were obtained from each RA, OA, or control group. Differences in the mean of each Wnt gene, β-catenin, FRZB, and LRP5 among experimental groups were evaluated with Dunnett's test.

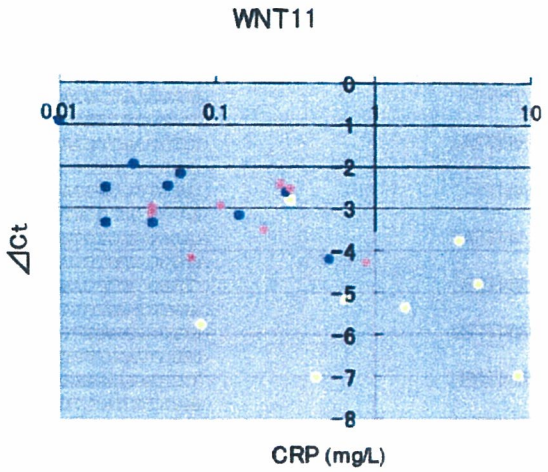

Figure 2. Clinical data of WBC count, CRP (mg/L), and Hct (%). Blue dots represent the data from control, pink dots from OA, and yellow dots from RA synovium. Wnt-11 expression significantly decreased as CRP increased in RA and OA patients, compared with control patients.

RNA Probes for in Situ *Hybridization*

A 354-base fragment of human Wnt-7b cDNA and a 402-base fragment of human Wnt-10a cDNA were subcloned into pBlueScript SK(−) vector (Stratagene, Tokyo, Japan) and used for generation of sense and antisense RNA probes. The sequences of Wnt-7b and Wnt-10a probes correspond to GenBank no. AB062766, position 1105 to 1458, and no. AB059569, position 1199 to 1600, respectively.

In Situ *Hybridization*

Three severe RA patients and three severe OA patients after TKA were used for histological assessment. A 49-year-old female RA patient after TKA (most severe case) and a 94 year-old male OA patient after TKA (most severe case), are shown here. After the operations, articular cartilage, bone, and synovial tissues were taken out *en bloc*, cut at 2 mm thickness, and fixed in fresh 10% neutral buffered formalin for 24 hours. The cartilage and bone tissues were decalcified with 20% EDTA after washing with 0.1 mol/L phosphate-buffered saline (PBS). They were then dehydrated through a graded ethanol series and embedded in paraffin. Sections of 4 μm thickness were cut and mounted on α-aminopropyl triethoxysilane (APS)-coated slides. They were stored at 4°C until use.

Sections were blow-dried, deparaffinized, rehydrated, and fixed with 4% paraformaldehyde for 10 minutes at room temperature. They were then successively treated with PBS for 5 minutes, 15 μg/ml proteinase (DAKO Cytomation, Cambridgeshire, UK) in PBS for 10 minutes at 37°C, 4% paraformaldehyde for 10 minutes, 0.2 N HCl for 10 minutes, 0.1 mol/L triethanolamine for 5 minutes, and 1% acetic acid/0.1 mol/L triethanolamine for 10 minutes. Digoxigenin (DIG)-labeled single-strand antisense RNA probes for Wnt-7b and -10a were prepared with a DIG-labeling Mix (×10 concentration). The histological sections were covered with siliconized coverslips and incubated at 60°C for

Table 1. Real-Time PCR Primers

Gene	Primer sequence	Probe
WNT3	GGAGAAGCGGAAGGAAAAATG	TTCCACTGGTGCTGCTACGTCA
	GCACGTCGTAGATGCGAATACA	
WNT3A	CCTGCACTCCATCCAGCTACA	AGAAGCCTCTCGTCCCGTCCCTCC
	GACCTCTCTTCCTACCTTTCCCTTA	
WNT4	GATGTGCGGGAGAGAAGCAA	AACCTCCACAACAATGAGGCCGGC
	ATTCCACCCGCATGTGTGT	
WNT5A	GAAATGCGTGTTGGGTTGAA	TTCTGCCTCACCCCTTTGTCT
	ATGCCCTCTCCACAAAGTGAA	
WNT5B	CTGCCTTTCCAGCGAGAATT	TCCACGGTTCACTAGCTCCTACCT
	AGGTCAAATGGCCCCCTTT	
WNT7B	CCCGGCAAGTTCTCTTTCTTC	AGCAAAGTGATGAGGAGACTGAGCGT
	GGCGTAGCTTTTCTGTGTCCAT	
WNT8B	TCCCAGAAAAACTGAGGAAACTG	CCCCGGAAAAGCATGTCTTTGGG
	AACCTCTGCCTCTAGGAACCAA	
WNT10A	GGCAACCCGTCAGTCTGTCT	CATCCTTTCACCCCTTCCCTG
	CATTCCCCACCTCCCATCT	
WNT10B	CTTTTCAGCCCTTTGCTCTGAT	TCTTGGTCCCTGGAAGCTTAAAGT
	CCCCTAAAGCTGTTTCCAGGTA	
WNT11	GGCTTGTGCTTTGCCTTCA	TTGGAAGCCACCAGGAACAGAAGG
	TTTGATGTCCTGCCCTCCTT	
WNT13	TGCCAAGGAGAAGAGGCTTAAG	CCCGGGCCCTCATGAACTTACA
	GTGCGACCACAGCGGTTATT	
WNT14	CTTAAGTACAGCAGCAAGTTCGTCAA	AGCAAGGATCTGCGAGCCCGTGT
	CCACGAGGTTGTTGTGGAAGT	
WNT15	CAGGTGCTGAAACTGCGCTAT	CTCGGCTGTCAAGGTGTCCAGT
	GCCCAAGGCCTCATTGGT	
β-Catenin		
F	5′-CTGCTGTTTTGTTCCGAATGTC	
R	5′-CCATTGGCTCTGTTCTGAAGAGA	
Probe	5′-AAACGGCTTTCAGTTGAGCTGACC	
FRZB	CCTGCCCTGGAACATGACTAA	CAACCACCTGCACCACAGCACTCA
	CAGACCTTCGAACTGCTCGAT	
LRP5		
F	5′-GCTGTACCCGCCGATCCT	
R	5′-GGCGCCATTCCTCGAAT	
Probe	5′-CAAACATTCCGGCCACTGCGAGAC	

All primer sequences are written from 5′ to 3′. For each primer pair, the top sequence is sense, and the bottom sequence is antisense.

16 hours in a humid chamber. The hybridization solution contained 50% deionized formamide, 5× standard saline citrate (SSC), 1% sodium dodecyl sulfate (SDS), 50 μg/ml of heparin, and approximately 75 ng/slide of RNA probe. After hybridization, the slides were washed two times for 10 minutes with 2× SSC at 50°C, and 0.2× SSC at 50°C. Hybridized DIG-labeled probes were detected by Tris-buffered saline (TBS) (0.3% Tween 20), blocking solution, anti DIG-alkaline phosphatase-labeled antibody (1:2000), TBS (0.3% Tween 20) twice, APB (0.1 mol/L Tris-HCl (pH 9.5), 0.1 mol/L NaCl, and 50 mmol/L $MgCl_2$) and then 4-nitroblue tetrazolium chloride/5-bromo-4-chloro-3-indolyl phosphate (NBT/BCIP) (Boehringer, Tokyo, Japan). Thereafter, the slides were mounted with Kernechtrot stain solution (Muto Chemical Co., Tokyo, Japan). The control procedures consisted of hybridization with the sense probes and omission of either antisense RNA probe or the anti-DIG antibody.

Hematoxylin and Eosin and Immunohistochemical Staining

Hematoxylin and eosin and immunohistochemical staining were performed with the same block used for *in situ* hybridization, and sections of 4 μm thickness were prepared using a microtome. Anti-human Wnt-7b and -10a antibodies were purchased from Sigma Genosys (Tokyo, Japan). Deparaffinized sections were treated with 0.3% hydrogen peroxide in methanol at room temperature for 30 minutes to quench endogenous peroxidase and then washed in TBS. The sections were treated with 0.05% proteinase K in TBS and then washed in TBS. They were incubated overnight at 4°C with rabbit anti-Wnt-7b or -10a antibody diluted to 2 μg/ml, after they were treated with normal goat serum for 30 minutes at 37°C to avoid nonspecific binding. After washing in TBS, they were incubated at room temperature for 30 minutes with a 1:600 Biotinylated goat anti-rabbit immunoglobulins (DAKO Cytomation). They were treated with peroxidase-conjugated streptavidin (Nichirei Co., Tokyo, Japan) at room temperature for 5 minutes and then washed in TBS. Color was developed by the DAB substrate kit (Nichirei Co., Tokyo, Japan). Finally, the sections were counterstained with hematoxylin. Control sections were treated in the same manner with 1% bovine serum used in place of the primary antibodies.

Examination of Clinical Data

Blood was taken from the patients before operations to obtain clinical data including white blood cell (WBC) count, C-reactive protein (CRP) (mg/L), and Hematocrit

(Hct) (%). Samples from the same patients described under "Tissue Collection and Processing for Real-Time PCR" were used here. The latest data from the patients before the surgeries are reported in the present study.

The correlation between expression level of Wnt gene and clinical data were examined. Every possible combination between the order of ΔCt value of Wnt and the order of clinical data value of tissue donor (WBC, CRP, Hct, and age) was tested with Spearman's Rank Correlation Method.

Cell Cultures, Plasmids, and Transfection Procedures

Considering that the expression of Wnt-7b was up-regulated in OA cartilage and RA synoviums at the mRNA and protein levels, compared with the controls, we next tried to investigate the function of Wnt-7b in those tissues.

Primary synovial cells and chondrocytes in control patients were generated for the following transfection as described previously.[24] Primary synovial cells and chondrocytes in RA and OA patients were also generated for the following Western blot analysis and cytokine assay. Cells were plated at 2×10^6 cells/100-mm plastic dish (Falcon #3003; Becton Dickinson Labware, Tokyo, Japan) in 10 ml of Dulbecco's modified Eagle's medium (DMEM; Gibco-BRL, Grand Island, NY) with 10% fetal calf serum (Sigma Chemical Co., St. Louis, MO) at 37°C and incubated for 1 day before transfection. Transfection grade eukaryotic expression vector containing hemagglutinin-tagged mouse Wnt-7b under the control of cytomegalovirus promoter was purified using standard procedures (Upstate Biotechnology, Lake Placid, NY). The amino acid homology of Wnt-7b between mouse and human is approximately 98% (GenBank human Wnt-7b, NP478679; mouse Wnt-7b, NP033554).

For each plate to be transfected, 4 μg of Wnt-7b plasmid with serum-free DMEM was combined with LipofectAmine plus reagent (Invitrogen, Carlsbad, CA) and then incubated at room temperature for 15 minutes. LipofectAmine reagent was also combined with serum-free DMEM and then added dropwise to a small Eppendorf tube containing DNA. After tapping to mix, the tubes were incubated at room temperature for 15 minutes. Without removing the overlying media from cells, the entire LipofectAmine reagent/DNA mixture was added dropwise to the plates. The plates were gently rocked to mix, and then incubated at 37°C, 5% CO_2. The following day, medium was replaced with 5 ml of serum-free DMEM. After an incubation of 24 hours, conditioned medium was collected and subject to Western blot analysis.

Western Blot Analysis

Because Wnt-7b is a secreted protein, 0.5 ml of supernatant from each plate was added to 0.5 ml of sample buffer (0.05 mol/L Tris-HCl (pH6.8), 2% SDS, 6% β-mercaptoethanol, and 10% glycerol) and centrifuged at 12,000 × *g* for 5 minutes at 4°C. Then the protein content of each sample was measured by a UV assay at an OD of 280 nm. Anti- Wnt-7b human antibody was used at a dilution of 1 μg/ml. Aliquots of protein solution (5 μl) were adjusted to 1 μg/μl, mixed with 1% bromophenol blue (1 μl; Sigma, St. Louis, MO), and then boiled for 2 minutes. They were then loaded on SDS (10% ~ 20%) acrylamide gradient gels (35 mA, low voltage, 90 minutes). The protein bands were transferred to a polyvinylidene difluoride membrane (Immunobilon-P Transfermembrane; Millipore, Bedford, MA) according to the manufacturer's instructions. After treatment with blocking reagent (Nippon Roche Co., Tokyo, Japan) for 1 hour at room temperature, the membranes were washed with PBS for 5 minutes and then incubated for 1 hour with primary antibody (1:200). After two 5-minute washes with PBS, the membranes were incubated with horseradish peroxidase (HRP)-conjugated rabbit anti-goat antibodies (1:500, Histofine; Nichirei Co.) for 1 hour. After two further 5-minute washes with PBS, the immunoblot was developed using an ImmunoStar kit for Rabbit (Wako Pure Chemical Industries Ltd., Tokyo, Japan) in the process of the detection of biotin and chemiluminescence. We used β-tubulin as an internal control.

Cytokine Assay

Because the expression of Wnt-7b was up-regulated in transfected RA synovial cells at the protein level, we next sought to examine how Wnt-7b would affect inflammatory cytokines tumor necrosis factor-α (TNF-α), interleukin (IL)-1β, and IL-6.

Human cytokine antibody arrays with TNF-α, IL-1β, and IL-6 were purchased from RayBiotech, Inc. (Tokyo, Japan). The supernatant from human primary synovial cells (RA, OA, control patients, and Wnt-7b transfected normal synovial cells) were placed into the array membrane. The array membranes were then washed with wash buffer after treatment with blocking buffer (5% BSA/TBS, 0.01 mol/L Tris-HCl, and 0.15 mol/L NaCl) and then incubated for 2 hours with biotin-conjugated anticytokine antibodies to remove unbounded cytokines. The membranes were incubated with HRP-conjugated streptavidin (2.5 pg/ml) for 60 minutes at room temperature. After further washes with wash buffer to remove any unbound materials, the signals were detected and quantitated by a chemiluminescence imaging device and enhanced chemiluminescence system (Amersham Pharmacia Biotech, Aylesbury, UK). The changes of the signals were compared with the control patients (fold change = 1). The mean of fold change cytokines with SD were obtained from performing the assay five times for each group. Differences in the mean of fold change cytokines between experimental groups were evaluated with Dunnett's test.

Results

RT-PCR

Wnt-3, -3a, -4, -5a, -5b, -7b, -8b, -9a,14, -9b,15, -10a, -10b, -11, -13, and FRZB were detected among Wnt-1, -2,

-3, -3a, -4, -5a, -5b, -6, -7a, -7b, -8a, -8b, -9a, -9b, -10a, -10b, -11, -13, -16, and FRZB in all RA, OA cartilage and synoviums by RT-PCR. Each Wnt gene and FRZB were detected in every RA, OA cartilage and synovium tissue by RT-PCR (data not shown). Then, real-time PCR was performed for quantitative assessment.

Expression Profiles of Some Wnts, FRZB, LRP5, and β-Catenin mRNA in RA, OA, and Normal Tissue by Real-Time PCR

Real-time PCR revealed the overall level of each Wnt family member in human joint tissues. The overall expression patterns were not very different in RA, OA, and control groups. (Figure 1, A and B). In RA patients, Wnt-7b was significantly up-regulated (5.62-fold, $P < 0.01$) in synovium, and Wnt-10a was significantly up-regulated (3.73-fold, $P < 0.05$) in cartilage, when compared with control tissues. Wnt-3, -10b, -11, and FRZB were down-regulated in synovium. In OA patients, Wnt-7b was significantly up-regulated (6.25-fold, $P < 0.01$) in cartilage. Wnt-3a, -5b, -15, and FRZB were down-regulated in synovium, and Wnt-3, -14, and FRZB were down-regulated in cartilage (Figure 1C). LRP5 was down-regulated in RA, OA synovium and cartilage. FRZB was also down-regulated in RA cartilage, and OA synovium and cartilage. β-Catenin mRNA level did not significantly change in RA or OA samples, compared with control tissues.

Examination of Clinical Data

Among every possible combination between the expression level of Wnt genes and clinical data, the most significant relationship was found between Wnt-11 and CRP (correlation, −0.64; $P < 0.001$). As shown in Figure 2, as CRP increased, the expression of Wnt-11 decreased.

In Situ *Hybridization Study*

As the expression of Wnt-7b and -10a increased in RA and/or OA groups, compared with the control groups, we next tried to find the localizations of those genes by *in situ* hybridization. *In situ* hybridization revealed that in RA patients, Wnt-7b was strongly expressed in the macrophage-like cells, fibroblastic cells, and vessel walls in the synovium, particularly in the region of inflammation. Wnt-10a was weakly expressed in chondrocytes of articular cartilage, bone marrow stromal cells, or hematopoietic cells in subchondral bone but strongly expressed in macrophage-like cells, fibroblastic cells, and vessel walls in the synovium. In OA patients, Wnt-7b was strongly expressed in chondrocytes, osteoclast-like cells in the osteophyte and articular cartilage, and bone marrow stromal cells or hematopoietic cells in subchondral bone. It was also strongly expressed in macrophage-like cells, fibroblastic cells, and vessel walls in the synovium, particularly in the region of inflammation. Wnt-10a was weakly expressed in chondrocytes, osteoclast-like cells in the osteophyte and articular cartilage, and bone marrow stromal cells or hematopoietic cells in subchondral bone. It was also expressed in macrophage-like cells, fibroblastic cells, and vessel walls in the synovium (Figure 3, A to F; Wnt-10a: data not shown).

Immunohistochemical Study and Western Blotting

An immunohistochemical study was performed on Wnt-7b and -10a, because of the significant up-regulation of these genes by real-time PCR and the expression of those genes by *in situ* hybridization in RA and/or OA joint tissues. In RA and OA joint tissues, Wnt-7b was heavily localized in macrophage-like cells, fibroblastic cells, and vessel walls in the synovium, weak and sparse chondrocytes in articular cartilage, bone marrow stromal cells, or hematopoietic cells in subchondral bone. Wnt-10a was not detected in joint tissue (Figure 3, A to F; Wnt-10a: data not shown). Western blotting analysis also confirmed that the expression of Wnt-10a was not detected at the protein level in RA and OA joint tissues (data not shown).

Transfection of Wnt-7b, Western Blotting Analysis, and Cytokine Assay

As the expression of Wnt-7b was enhanced in RA, OA joint tissues at mRNA and the protein levels, we further investigated the secretion of inflammatory cytokines after transfection of Wnt-7b in control chondrocytes and synovial cells. LipofectAmine reagent transfected approximately 10% of the undifferentiated mesenchymal cells confirmed by Western blotting and immunohistochemistry (data not shown).

Western blotting analysis revealed that the secretion of Wnt-7b in the transfected synovial cells in control patients was similar to that of synovial cells in RA patients (Figure 4). The secretion of Wnt-7b in the transfected cartilage cells in control patients was not detected (data not shown).

Compared with the empty vector transfected controls, the secretion of TNF-α, IL-1β, and IL-6 in primary synovial cells of OA patients were not significantly changed. However, the secretion of TNF-α, IL-1β and IL-6 in primary synovial cells of RA patients and the Wnt-7b transfected normal synovial cells, especially TNF-α, significantly increased the expression level twofold to fourfold ($P < 0.05$) (Figure 5).

Discussion

The etiopathogenesis of RA or OA is still the subject of intense debate and research. This is the first comprehensive study of all known human Wnt genes and the Wnt-related genes, β-catenin, FRZB, and LRP5 in joint tissues from human RA and OA patients. Compared with normal tissues, real-time PCR revealed that Wnt-7b in OA cartilage and RA synoviums and Wnt-10a in RA cartilage were

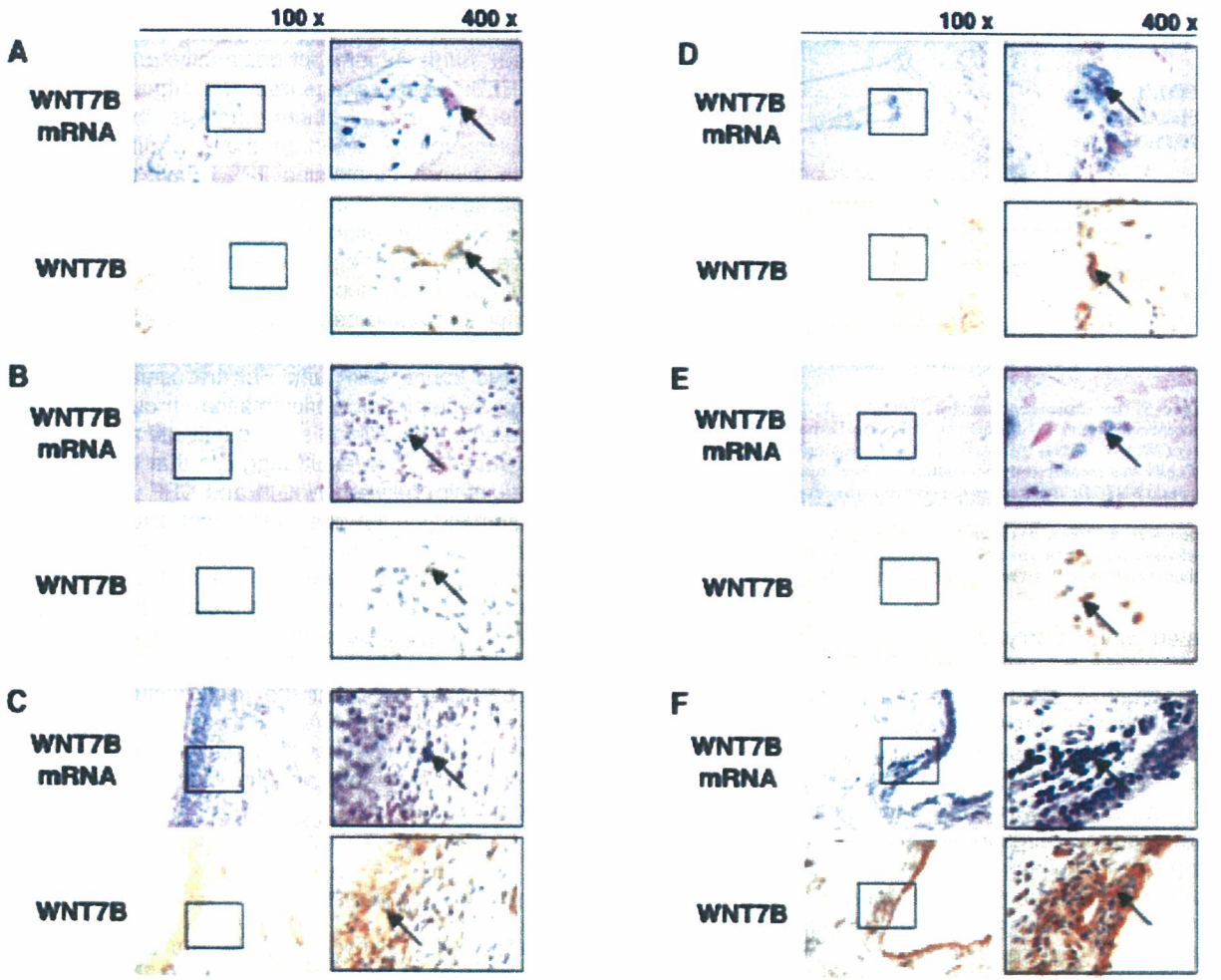

Figure 3. Histological appearance of Wnt-7b by *in situ* hybridization (ISH) and immunohistochemistry (IHC). Cross-section at 100× magnification is in the **left panel** and 400× magnification section is in the **right panel**. Higher-magnification images corresponding to the box areas in each figure. In RA samples, ISH and IHC show that Wnt-7b is present at osteoclast-like cells of articular cartilage (**A**, **arrows**), bone marrow stromal cells or hematopoietic cells of bone marrow (**B**, **arrows**), and fibroblastic cells and vessel walls of the synoviums (**C**, **arrows**). In OA samples, ISH and IHC reveal that Wnt-7b is expressed in multinucleated osteoclast-like cells in osteophytes (**D**, **arrows**), osteoclast-like cells in the articular cartilage (**E**, **arrows**), and fibroblastic cells and vessel walls of synovium (**F**, **arrows**).

significantly up-regulated at mRNA level. An *in situ* hybridization study revealed that in OA patients, Wnt-7b and -10a were expressed in chondrocytes or osteoclast-like cells in osteophytes, chondrocytes in articular cartilage, bone marrow stromal cells or hematopoietic cells in subchondral bone, and fibroblastic cells and vessel walls in the synovium. In RA patients, Wnt-7b was expressed in chondrocytes in articular cartilage, bone marrow stromal cells or hematopoietic cells in subchondral bone, and

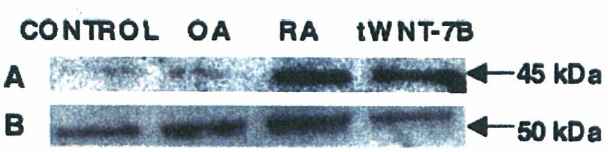

Figure 4. Western blot analysis of Wnt-7b using primary synovial cells in control, RA, OA patients, and normal synovial cells after transfection of Wnt-7b (tWNT-7B). The expression of Wnt-7b was significantly increased in RA and tWNT-7B, compared with the control and OA samples (**A**). β-Tubulin protein levels obtained by Western blotting was used as a positive control (**B**).

fibroblastic cells and vessel walls in synovium. Wnt-10a was expressed in chondrocytes of articular cartilage and bone marrow stromal cells or hematopoietic stem cells in subchondral bone. Wnt-10a was also expressed in fibroblastic cells and vessel walls in synovium. However, Wnt-10a was not detected at the protein level. Therefore, the increased expression of Wnt-7b may be a relationship with joint disease in RA and OA patients. Wnt-7b was transfected into primary chondrocytes and synovial cells in control patients to elucidate the role of RA or OA. We then investigated the secreted levels of TNF-α, IL-1β, and IL-6 in those cells. As a result, the secretion of TNF-α, IL-1β, and IL-6 in primary synovial cells of RA patients and the Wnt-7b transfected normal synovial cells were significantly enhanced compared with the control tissues. These results suggest that the expression of Wnt-7b in RA synovium might play a few roles in the process of RA inflammation. The reason why Wnt-7b was expressed in vessel walls in RA and OA synoviums is still unclear. However, the results might indicate that Wnt-7b is asso-

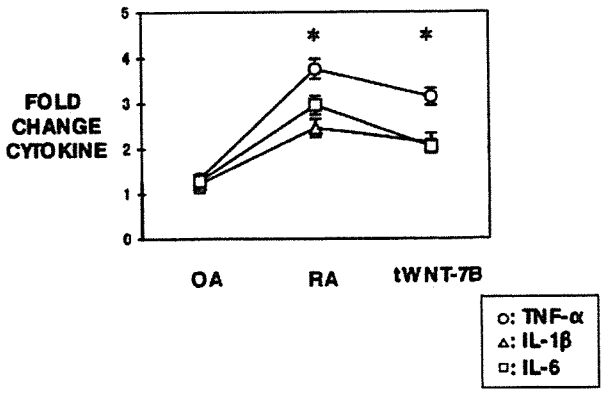

Figure 5. The expression changes of TNF-α, IL-1β, and IL-6 in primary synovial cells from RA, OA patients, and normal synovial cells after transfection of Wnt-7b (tWNT-7B). Quantitation of cytokine levels in primary synovial cells was measured by chemiluminescence imaging device in the OA, RA, and tWNT-7B. The score in the controls (the expression in empty vector transfected cells) was used as a standard (fold change of controls = 1). The expression of TNF-α, IL-1β, and IL-6 in RA, and tWNT-7B was twofold to fourfold changes than that of OA. The expression of TNF-α was significantly higher than that of IL-1β and IL-6 in each group ($P < 0.05$).

ciated with not only with joint destruction, but also perhaps within the vessel walls. Wnt-7b was expressed in bone marrow stromal cells or hematopoietic cells in RA and OA bone marrow tissues, however, the cells were not specified. Further studies would be necessary to clarify the localization of Wnt-7b in joint tissues.

Osteophytes, which are most notably present at the joint margins, represent areas of new cartilage and bone formation in humans and have been used to characterize OA. The presence of osteophytes, which can distinguish OA from RA, has commonly been used in the definition of OA.[2,3,24,25] It seems likely that mechanical, humoral, and other factors are involved in stimulating the formation of osteophytes, although the cause of growth and development of osteophytes remains unclear. In this study, Wnt-7b in OA cartilage was significantly up-regulated by real-time PCR. At mRNA and protein levels, Wnt-7b was expressed in cartilage cells or osteoclast-like cells in osteophytes and bone marrow stromal cells or hematopoietic cells in subchondral bone. Therefore, Wnt-7b might affect osteophyte formation.

There are three pathways in Wnt signaling. The Wnt-β-catenin cascade is thought to be the main pathway.[26–28] β-Catenin is the key mediator of the Wnt signal and is usually stored in the cytoplasm. Wnt-1, -8a, and -8b are involved in the Wnt-β-catenin cascade as described previously.[29–30] Here, Wnt-8b was significantly down-regulated in OA synovium, compared with normal synovium, although the expression of β-catenin did not significantly change in OA or RA tissue, compared with normal tissues, by real-time PCR. These results suggest that Wnt-β-catenin signaling might not be involved in human joint destruction. Functional investigations would be necessary to support these results. LRP5 is capable of functioning in the Wnt/β-catenin signaling pathway.[29] Wnt/LRP5 signaling is necessary for the induction of alkaline phosphatase, and the Wnt/β-catenin signaling pathway can act in a Smad-independent manner in ST2 cells and C3H10T1/2 cells.[30] The down-regulation of LRP5 mRNA in OA or RA tissue in this study, compared with normal tissues, might suggest that LRP5 is not activated during human joint destructive processes.

FRZB, which antagonizes Wnt signaling, appears to indirectly promote chondrogenesis by removing the blocking activity of Wnt on chondral differentiation. Cartilage extracts containing FRZB have *in vivo* chondrogenic activity.[31–33] In our study, FRZB was down-regulated in OA synovium and cartilage and in RA cartilage. Therefore, FRZB might be also involved in human joint cartilage destruction. FRZB is also a member of Wnt family, so it would be important to look at the expression of FRZB-related genes in these tissues.

WBC count, CRP, and Hct are useful parameters to judge systemic joint inflammation. In our study, as CRP increased, only Wnt-11 significantly decreased in RA and OA patients. This result suggests that there might be a relationship between Wnt-11 and CRP in the process of inflammation in the destructive joint disease.

In conclusion, our results suggest that Wnt signaling mechanisms are involved in the joint pathology associated with RA and OA disease progression. The secretion of Wnt-7b might be a key factor in inflammation of RA. Therefore, the regulation of Wnt expression may provide opportunities to arrest the joint destruction and pain linked with RA and OA. Future studies will be directed toward understanding the relationship between Wnt genes, Wnt receptors, and the effectors of Wnt signaling in joint tissues.

Acknowledgments

We thank Dr. Hiroyuki Nakaya and Dr. Hiroshi Ota at Department of Orthopaedic Surgery, Shinshu University School of Medicine, and Dr. Takahiro Nomura at Iida Municipal Hospital for providing us with various human tissue samples. We are grateful to Dr. Jun Ishizaki and Dr. Etsuo Nakamura at Shionogi & Co. Ltd, for their technical assistance and valuable discussion. We also thank Dave C. Morris of Discovery Research Biology and Simone Wilson at Case Western Reserve University for their writing assistance. All research was performed at Shinshu University School of Medicine.

References

1. Haugeberg G, Orstavik RE, Kvein TK: Effects of rheumatoid arthritis on bone. Curr Opin Rheumatol 2003, 15:469–475
2. Moskowitz RW, Howell DS, Altman RD, Buckwalter JA, Goldberg VM: Osteoarthritis, ed 3. Diagnosis and Medical/Surgical Management, Philadelphia: W.B. Saunders, 2003
3. Hashimoto S, Creghton-Achermann, Takahashi K, Amiel D, Coutts RD: Development and regulation of osteophyte formation during experimental osteoarthritis. Osteoarthritis Cartilage 2002, 10:180–187
4. National Center for Health Statistics, Centers for Disease Control and Prevention, US Department of Health and Human Services. National Health and Nutrition Examination Survey, III 1988–1994. Hyattsville, MD, Division of Data Services, National Center for Health Statistics, US Centers for Disease Control and Prevention, 1996
5. Grotewold L, Ruther U: Bmp, Fgf and Wnt signalling in programmed cell death and chondrogenesis during vertebrate limb development: the role of Dickkopf-1. Int J Dev Biol 2002, 46:943–947